

## Electronic and Molecular Structures of the CeB<sub>6</sub> Monomer

Jarrett L. Mason<sup>†</sup>, Hassan Harb<sup>‡</sup>, Caleb D. Huizenga<sup>†1</sup>, Joshua C. Ewigleben<sup>†</sup>, Josey E. Topolski<sup>†</sup>, Hrant P. Hratchian<sup>\*‡</sup>, and Caroline Chick Jarrold<sup>\*†</sup>

<sup>†</sup>*Department of Chemistry, Indiana University, 800 E. Kirkwood Ave, Bloomington, IN, 47405,*

<sup>‡</sup>*Department of Chemistry and Chemical Biology, University of California, Merced, 5200 North Lake Road, Merced, CA 95343*

### ABSTRACT

The electronic and molecular structure of the CeB<sub>6</sub> molecular unit has been probed by anion PE spectroscopy and DFT calculations to gain insight into structural and electronic relaxation on edge and corner sites of ionic material. While boron in bulk lanthanide hexaboride materials assumes octahedral B<sub>6</sub><sup>3-</sup> units, the monomer assumes a less compact structure to delocalize the charge. Two competitive molecular structures were identified for the anion and neutral species, which include a boat-like structure and a planar or near-planar teardrop structure. Ce adopts different orbital occupancies in the two isomers; the boat-like structure has a 4*f* superconfiguration while the teardrop favors a 4*f*6*s* occupancy. The B<sub>6</sub> ligand in these structures carries a charge of -4 and -3, respectively. The teardrop structure, which was calculated to be isoenergetic with the boat structure, was most consistent with the experimental spectrum. B<sub>6</sub>-local orbitals crowd the energy window between the Ce 4*f* and 6*s* (HOMO) orbitals. A low-lying transition from the B-based orbitals is observed slightly less than 1eV above the ground state. The results suggest that edge and corner conductivity involves stabilized, highly diffuse 6*s* orbitals or bands rather than the bulk-favored 5*d* band. High-spin and open-shell low-spin states were calculated to be very close in energy for both the anion and neutral, a characteristic that reflects how decoupled the 4*f* electron is from the B<sub>6</sub> 2*p*- and Ce 6*s*-based molecular orbitals.

<sup>1</sup> Current Address: Grand Valley State University Department 1 Campus Drive, 312 Padnos Hall, Allendale, Michigan 49401

## I. INTRODUCTION

Lanthanide borides possess a range of interesting electronic and magnetic properties,<sup>1</sup> beyond the common usage of LaB<sub>6</sub> as an emitter used in electron guns. CeB<sub>6</sub> in particular, which is also used as an emitter, is a heavy fermion material, and has temperature dependent and “hidden” magnetic phases. Structurally, these materials are cluster compounds, in which boron units assume the form of B<sub>6</sub><sup>3-</sup> octahedra with the Ln<sup>3+</sup> cations arranging in CsCl-like packing.<sup>2,3</sup> In tetraboride crystals, the octahedra are connected by boron dimers, and form channels filled by Ce atoms.

Fundamentally, the complex electronic and magnetic properties of lanthanide based materials arise from partially-filled but contracted core-like 4*f* orbitals. While the 4*f* orbitals are generally considered to be core-like and non-bonding, they lie close in energy to the 5*d* and 6*s* valence electrons, giving rise to a constellation of very close-lying electronic states resulting from a single general subshell occupancy, or “superconfiguration,” to borrow a term from seminal work on the lanthanide oxide diatomics.<sup>4-18</sup> As an example, the two singly occupied orbitals in the CeO neutral diatomic can be largely described as Ce-local 4*f* and 6*s* orbitals, the latter being very delocalized and therefore modestly antibonding; there are 16 very close-lying electronic states arising from this 4*f* 6*s* superconfiguration.<sup>19</sup> From a molecular standpoint, there have been very few electronic spectroscopic studies on lanthanide oxides larger<sup>20</sup> than diatomic molecules (a sampling is included in the references cited)<sup>4-18</sup> let alone borides, aside from several recent anion photoelectron spectroscopic studies, including new and interesting “inverse-sandwich” complexes consisting of planar boride rings sandwiched by lanthanide cations.<sup>21-26</sup> In particular, the studies by Wang and coworkers on Pr-doped B<sub>x</sub> clusters (*x* = 3, 4, 7) provide a story of structural evolution with increasing B coordination.<sup>23,27</sup>

Since bonding in ionic systems is localized, and in the case of lanthanide borides, the material itself is cluster-like, small cluster models provide a particularly powerful platform for probing the electronic and molecular structures, both from a computational/theoretical standpoint, as well as experimentally owing to the accessibility of mass selected clusters of these systems and their spectroscopic characterization. The molecular and electronic structures of clusters are governed by the same attributes that govern bulk properties, as supported by numerous studies on elemental and ionic cluster systems across the periodic table.<sup>28-34</sup>

Recently, Bowen and coworkers reported the anion PE spectrum of  $\text{SmB}_6^-$ . Electron detachment energies were calculated using the CASPT2 method, and Kohn-Sham orbitals were used to model the detachment process.<sup>21</sup> While they were unable to definitively assign the structure based on the calculations, a near planar  $C_{2v}$  structure was consistent with their spectrum. The spectrum appeared to be congested with numerous, overlapping electronic transitions, making assignments particularly challenging. The Sm center in bulk  $\text{SmB}_6$  has a  $4f^5$  subshell occupancy, and nominally the same was found in calculations on the molecular unit, though there was some delocalization of the  $4f$  electrons into the  $2p$  molecular orbitals predicted, which is contrary to the general viewpoint of the core-like character of the  $4f$  subshell. The near-half-filled subshell does result in exceptionally complex electronic structure. However, a similar study on  $\text{LiB}_6^-$  photoelectron spectrum with attending theoretical treatment by Wang and coworkers was similarly complex, with an anion PE spectrum as congested as the  $\text{SmB}_6^-$  spectrum. Calculations on  $\text{LiB}_6^-$  suggested a  $\text{B}_6^{2-}$  ring complexed to the  $\text{Li}^+$  cation, with all the detachment transitions being associated with  $\text{B}_6^{2-}$  orbitals.<sup>35</sup>

$\text{CeB}_6^-$  offers a molecule with interactions between the metal center and the boron cluster that is comparable to  $\text{SmB}_6^-$ , but should be simpler from a computational standpoint, since the  $4f$

subshell would at most be singly occupied. Based on the comparison of a large number of calculated structures with photoelectron angular and vibrationally resolved anion PE spectra reported in this paper, the molecular unit assumes a planar  $C_{2v}$  or near-planar  $C_s$  structure, that can be described as  $Ce^{2+}(B_6)^{3-}$  for the anion and  $Ce^{3+}(B_6)^{3-}$  for the neutral. We compare the relative energy of more bulk-like unit structures to the planar structure determined from the spectrum, and relate the findings to what would likely be structural changes in the bulk  $(B_6)^{3-}$  octahedral units located on edges or corners, and the impact on the electronic structure and emission properties.

## II. METHODS

$CeB_6^-$  molecular anions were produced, mass separated in a time-of-flight (TOF) mass spectrometer, and probed by PE spectroscopy using an apparatus that has been described previously;<sup>36,37</sup> A brief description follows.  $CeB_6^-$  and a wide range of other  $Ce_xO_yB_z^-$  species, were produced using a pulsed laser ablation source in which a rotating  $CeB_6$  rod (QS Rare Elements 99%) was ablated by the second harmonic output of a Nd:YAG laser (532 nm, 2.33 eV) operating at a repetition rate of 30 Hz. A pulse of high pressure ultra-high purity He carrier gas introduced by a solenoid-type molecular beam valve swept the resulting plasma through a coupling piece similar to the design of Dietz et al.,<sup>38</sup> into a 25-mm long, 3-mm diameter clustering channel. After expanding into a vacuum chamber, the gas mixture was collimated as it passed through a 3 mm skimmer. Anions were then accelerated to 1 keV and entered a 1.2 m beam-modulated TOF mass spectrometer. Ions collided with a microchannel plate detector assembly at the end of the field free drift region.

Before colliding with the ion detector,  $CeB_6^-$  was selectively photodetached with the second (532 nm, 2.330 eV) or third (355 nm, 3.495 eV) harmonic output of a second Nd:YAG laser. A second microchannel plate detector assembly detected the small fraction of the detached

electrons that travelled the length of a 1-m field-free drift tube, perpendicular to the ion beam drift tube. The drift times were recorded with a digitizing oscilloscope, accumulating signal over  $2.52 \times 10^6$  laser shots with 2.330 eV photon energy, and  $3.36 \times 10^6$  laser shots for 3.495 eV photon energy, at each laser polarization (*vide infra*). The drift times were converted to electron kinetic energy,  $e^-KE$ , by calibrating with the well-known spectra of  $O^-$  and  $OH^-$ . While the target was in the vacuum chamber, minor oxidation of the target after several weeks of data collection became evident from the appearance of detachment signal from the mass-coincident  $CeO_2B_3^-$  ion, the spectrum of which had been reported previously.<sup>22</sup> The  $CeO_2B_3^-$  signal was subsequently subtracted from the spectra shown below.

The spectra presented below are plotted as a function of electron binding energy,  $e^-BE$ , which is related to the photon energy ( $h\nu$ ) by:

$$e^-KE = h\nu - EA - E_{int}^{neutral} + E_{int}^{anion} = h\nu - e^-BE \quad (1)$$

$EA$  is the neutral electron affinity,  $E_{int}^{neutral}$  is the internal energy of the neutral (electronic, vibrational and rotational energy), and  $E_{int}^{anion}$  is similarly the internal energy of the anion, which is taken to be nearly zero. As a consequence, the  $e^-KE$  distribution observed reflects energy levels of in the neutral.

Spectra were collected with detachment laser polarization either parallel ( $\theta = 0^\circ \pm 10^\circ$ ) or perpendicular ( $\theta = 90^\circ \pm 10^\circ$ ) to the direction of electron detection, to approximate the anisotropy parameter,  $\beta$ ,

$$\beta = \frac{(I_0 - I_{90})}{(0.5I_0 + I_{90})} \quad (2)$$

which is 0 for isotropic photoelectron angular distributions, 2 for distributions that are parallel to the laser polarization, and  $-1$  for distributions that are perpendicular to the polarization. In

molecular systems, this value can give insight into the nature of the molecular orbitals from which the electrons are being detached.

**Computational Methods** Release and local development versions of the GAUSSIAN 16 quantum chemistry package were used to test the viability of a plethora of molecular and electronic structures of  $\text{CeB}_6^-$  and  $\text{CeB}_6$ .<sup>39,40</sup> The unrestricted B3LYP hybrid density functional method was used. The Stuttgart relativistic small core atomic natural orbital basis set and corresponding effective core potential (ANO/ECP) basis set with 28 core electrons and a contracted Gaussian basis for the valence electrons (14s 13p 10d 8f 6g)/[6s 6p 5d 4f 3g] was used for Ce,<sup>41</sup> and a Dunning-style correlation consistent basis set for the B atoms.<sup>42</sup> A wide range of isomers in numerous spin states were calculated, and vibrational analyses were performed to ensure structures were at local minima. The relative energies of the plethora of anion and neutral structures and spin states reported are zero-point energy corrected values. The Natural Ionization Orbital (NIO) model has been used to provide an orbital picture of the electron detachment process.<sup>43</sup>

In all cases, the stability of KS determinants has been verified.<sup>44,45</sup> The electronic structures of all converged Kohn-Sham DFT determinants have been fully characterized as part of our standard analysis. For the systems studied in this work, such a process requires special attention as multiple stable electronic configurations can be optimized with standard SCF optimization approaches. Of particular concern was ensuring that located electronic configurations resulted in anion/neutral electronic structure pairings corresponding to allowed one-electron transitions. In addition to manual inspection of each SCF solution obtained in our calculations, NIO analysis assisted with such concerns and, in some cases, was used to identify improved sets of orbitals for the SCF engine's initial guess.

The calculation of electronic excited states was carried out using the linear response form of time-dependent DFT.<sup>46-47</sup> Such calculations were carried out using optimized ground state geometries. The nature of each excitation was characterized using the Natural Transition Orbital (NTO) model of Martin.<sup>48</sup> To ensure convergence of the Davidson diagonalization process, TDDFT results reported below requested 30 states.

To compare computational and experimental results, the adiabatic and vertical detachment energies (ADE and VDE) of each anion was computed. The ADE is the difference between the zero-point corrected energies of the anion and one-electron accessible neutral with the common structure, and the VDE is the difference between the ground state energy of anion and single-point energy of neutral confined at anion geometry. Furthermore, spectral simulations were generated using spectroscopic parameters extracted from the computational output files using home-written codes that use structures and normal coordinates of the anion and neutral species as inputs.<sup>49</sup> Vibrational wavefunctions were approximated as harmonic oscillator wavefunctions, and the parallel approximation was assumed.

### III. RESULTS AND ANALYSIS

Figure 1 shows the PE spectra collected for  $\text{CeB}_6^-$  with (a) 2.330 and (b) 3.495 eV photon energies with laser polarization parallel (dark green and blue traces) and perpendicular (light green and blue traces) to the direction of electron detection. The spectra show an intense band exhibiting partially resolved vibrational structure with irregular spacing in both spectra, with an onset at approximately 1.36 eV. The feature is tentatively labeled to indicate two transitions, **x** and **X**, with **x** being much narrower than other features in the 1.3 eV to 1.7 eV  $e^-BE$  range. Both bands **X** and **x** are parallel transitions with  $\beta = 1.1(1)$ , consistent with detachment from a Ce-local 6s-like molecular orbital.<sup>11,13,14,22</sup> An additional broad feature, labeled **A**, with

isotropic photoelectron angular distribution is observed with a vertical detachment energy (VDE) of 2.28 eV. The origin of band **A** is difficult to identify because of the continuum signal observed from band **X** to higher  $e^-BE$ . This band is assigned to detachment of an electron nominally from the hexaboride unit, since detachment of a  $4f$  electron is expected to have a very small cross section.<sup>50</sup>

Computationally, two general structural isomers were found to be energetically competitive: A planar or near-planar teardrop structure, and a boat-like structures in which the  $B_6$  cluster assumes a structure comparable to the boat conformation of cyclohexane, with the Ce center serving as a mast. Figure 2 shows these structures and relative energies of several spin states of anions (bottom half) and neutrals (top half). Optimized geometries for these species along with a more comprehensive figure showing all converged structures is included in the [Supporting Information](#). Table 1 summarizes the relative energies, a general description of the electronic structures, and the  $\langle S^2 \rangle$  values.

The lowest energy  $CeB_6^-$  structure features a distorted boat-like  $B_6$  unit coordinated to a Ce center, in a pure doublet spin state. The geometry of this molecule is trivially distorted from  $C_2$  symmetry. A similar structure with  $C_{2v}$  symmetry lies 0.57 eV higher in energy. Within the accepted error of the computational model chemistry, a planar  $C_{2v}$  teardrop structure in a quartet spin state was found to be only 0.01 eV above the lowest lying boat structure. Several open-shell anion doublet spin states were also identified within 0.1 eV of the quartet state (*vide infra*). The lowest energy detachment transition associated with the boat structure is 1.74 eV. In better agreement with experimental observation, the lowest energy detachment for the teardrop structure is calculated at 1.52 eV.

We note that an anion structure most similar to the bulk, which is a Ce center coordinated to the face of a B<sub>6</sub> octahedron ([Supporting Information](#)), converged over 1.7 eV higher in energy. Isolated B<sub>6</sub> in neutral, anionic and dianionic charge states are predicted to be planar, with anion PE spectra of B<sub>6</sub><sup>-</sup> supporting the computational results for the neutral and anion.<sup>51</sup> A comparison of the electronic structures of the more bulk-like structure to the teardrop structure is included in the [Supporting Information](#).

Based on the orbital occupancies of the asymmetric boat structure, the anion can be described as Ce<sup>3+</sup>(B<sub>6</sub>)<sup>4-</sup>, with the hexaboride cluster being closed shell and the Ce center having a 4*f* occupancy. A higher lying quartet state with this structure can be described as Ce<sup>2+</sup>(B<sub>6</sub>)<sup>3-</sup>, with the Ce center having 4*f*6*s* occupancy, and the hexaboride cluster in a doublet state. The lowest energy electronic states of the neutral boat structure are accessed from the ground electronic state of the anion by detaching an electron from the hexaboride ligand Ce<sup>3+</sup>(B<sub>6</sub>)<sup>3-</sup>, which can yield open-shell singlet or triplet states, associated with antiparallel and parallel alignment of the two unpaired electrons. The calculations predict the open shell singlet energy to be only slightly lower than the triplet energy. The proximity of these two states suggests that the unpaired electrons in the Ce-local 4*f* orbital and the B<sub>6</sub>-local orbital are weakly (spin) coupled. Simulations of the <sup>1</sup>A ← <sup>2</sup>A and <sup>3</sup>A ← <sup>2</sup>A transitions generated from the computational results are shown in Figure 3(a). Both transitions are fairly vertical, with the short 264 cm<sup>-1</sup> vibrational progressions associated with the Ce–B<sub>6</sub> metal-ligand stretch.

The teardrop structure of the anion has a different occupancy, which can be described as Ce<sup>2+</sup>(B<sub>6</sub>)<sup>3-</sup>, with the Ce center having a 4*f*6*s* orbital occupancy and the hexaboride unit in a <sup>2</sup>A<sub>2</sub> state. Again, the 4*f* electron generally is decoupled from the other unpaired electrons, and the anion can assume pure quartet spin and open shell doublet spin states featuring anti-parallel

electrons occupying Ce  $4f$  and  $6s$  like orbitals. Furthermore, with five nearly degenerate  $4f$  orbitals, calculations on states with the single electron occupying different  $4f$  orbitals (symmetry broken by the  $B_6$  ligand) are very close in energy. Two examples of open shell doublet states that differ only by the symmetry of the singly occupied  $4f$  orbital are included in Table 1.

The lowest energy state of the neutral can be described as  $Ce^{3+}(B_6)^{3-}$ , with the Ce center having  $4f$  orbital occupancy and the hexaboride unit having a singly occupied  $p_\pi$  orbital. Calculations identified both high-spin triplet and low-spin open-shell singlet configurations of the neutral. In both cases, the planar  $C_{2v}$  neutral teardrop structures have one imaginary frequency, with the minimum energy puckered teardrop structure with  $C_s$  symmetry, similar to the structure of  $AlB_7^-$  cluster,<sup>52</sup> lying  $\sim 370\text{ cm}^{-1}$  lower in energy. This difference is sufficiently low to raise the possibility that, on average, the neutral geometry could be considered planar.

Notably the spin-squared expectation value for the open-shell singlets were all roughly 1.0, suggesting that the spin contaminated determinants can be characterized as equal admixtures of pure singlet and triplet determinants.<sup>53</sup> Previous work on metal oxides by our labs has demonstrated that in some cases spin contaminated results pose significant challenges for spectral analyses and that such cases can be improved using spin-projection methods.<sup>54,55</sup> With this in mind, geometry optimizations and analytic frequency calculations using the approximate projection (AP) model were carried out on these species.<sup>56-60</sup> The result of these calculations indicated that spin contamination has a small effect on the spectral analysis of the  $CeB_6$  teardrop. AP energy corrections are less than 0.01 eV, and AP calculations provide negligible changes to geometries force constants relative to the open-shell results.

Figure 3 includes simulations based on transitions from the quartet (**X**) and open-shell doublet anions (**x**) to the (b) triplet neutral and open-shell singlet confined to the planar structure

and (c) the triplet neutral and open-shell singlet allowed to relax. Note that the transition energies in both panels are very similar because of the very small relaxation energy of the neutral. Their profiles are slightly different, with the progression in the Ce-B<sub>6</sub> stretch (305 cm<sup>-1</sup> for the planar structure, 309 cm<sup>-1</sup> for the relaxed structure) being more extended for the planar teardrop structure, and the activation of the 73 cm<sup>-1</sup> pucker mode adding congestion to the profile for the simulation for the relaxed neutral structure. Figures 3(d) and (e) show the simulations with all origins shifted to modestly lower  $e^-BE$  to overlay the simulated spectra with the experimental spectrum (0.12 eV for the planar structure simulations, 0.07 eV for the relaxed structure simulations). All of the spectroscopic parameters extracted from the output files and used to generate the simulations are summarized in the [Supporting Information](#).

While we are unable to definitively assert whether the structure is puckered or, on average, planar, the simulations based on the teardrop structures are in better agreement with the observed spectrum than the boat structure. Recall that the anionic boat and teardrop structures have a fundamentally different orbital occupancy, with the boat structure having more negative charge carried by the (B<sub>6</sub>)<sup>4-</sup> unit compared to the (B<sub>6</sub>)<sup>3-</sup> planar unit of the teardrop. Figure 4 shows the NIOs associated with the lowest energy one-electron transitions from the ground states of the boat and teardrop structures. The NIO analysis clearly shows that detachment from the doublet anion state of the boat structure involves an orbital that is highly delocalized through the B<sub>6</sub> boat; detachment from the quartet anion involves a diffuse Ce 6s like orbital that also includes very modest  $\sigma$  bonding character with the adjacent B atoms. In all cases, the photoelectron in the teardrop structures involves the Ce 6s like orbital. The fact that the boat and teardrop structures are predicted to be isoenergetic suggests competition between Coulombic stabilization and the particular stability of planar boron cluster structures.<sup>61</sup> In the boat structure, the

negative charge spread over the  $(\text{B}_6)^{4-}$  unit is more wrapped around the  $\text{Ce}^{3+}$  center, maximizing the Coulombic stabilization of this ionic compound. The HOMO of the teardrop structure of the anion is a diffuse Ce  $6s$ -like orbital, which allows for a more stable planar structure of the  $\text{B}_6$  unit.<sup>51</sup>

Finally, we note that band **A**, which lies under 1 eV above bands **X** and **x**, exhibits an isotropic PAD, and is less intense than band **X**, suggesting that this detachment transition is likely associated with the hexaboride unit, resulting in a  $\text{Ce}^{2+} (4f 6s) (\text{B}_6)^{2-}$  neutral. In addition, this band is embedded in a rising continuum, suggesting strong vibronic coupling between the ground state and the low-lying  $\text{Ce}^{2+} (4f 6s) (\text{B}_6)^{2-}$  states. TDDFT calculations were carried out to explore this possibility. As shown in the [Supporting Information](#), excited electronic states were characterized using the NTO model. A neutral excited state corresponding to a transition from a Ce  $6s$  like orbital to a hexaboride based  $\pi$  orbital was located roughly 1.4 eV above the neutral ground state. Detachment from the anion to this neutral excited state would correspond to detachment of a photoelectron from the singly occupied  $\text{B}_6$  localized  $p_\pi$  orbital.

Figure 5 shows a schematic of the orbital energies and occupancies of  $\text{CeB}_6^-$ , with green boxes indicating Ce  $6s$ -like MOs, the orange lines indicating B  $2p$ -based MOs, the blue indicating O  $2p$ -based orbitals, and red lines indicating Ce  $4f$  orbitals. To indicate single occupation of orbitals in the schematic, the widths lines representing singly occupied orbitals are half that of doubly occupied orbitals. Unlike cerium oxide molecules in which there is a pronounced energy interval between the  $4f$  and  $6s$  orbitals similar to that in the bulk cerium oxide band structure, there are four B  $2p$  orbitals crowded between the  $4f$  orbital and the  $6s$  orbital in  $\text{CeB}_6^-$ . To further underscore the relative high energy of the B  $2p$  orbitals, schematics of the orbital energies and occupancies of  $\text{Ce}(\text{B}_3\text{O}_2)^-$ ,  $\text{Ce}(\text{BO})_2^-$ , and  $\text{CeO}^-$  are included for

comparison. Therefore, the low-lying excitations in neutral CeB<sub>6</sub> are expected to involve promotion from the pool of electrons in close-lying B 2*p* orbitals into the Ce 6*s* orbital. As will be discussed below, this is evocative of the thermal conductivity of the bulk material.

#### IV. DISCUSSION

The goal of this study was to determine how the electronic and molecular structure of the ionic CeB<sub>6</sub> cluster differed from the bulk material, as a way of gaining insight into structural and electronic relaxation on edge and corner sites. Our results suggest that the general charge separation between the Ce centers and the hexaboride clusters are similar in molecular units and the bulk, though the structures of the hexaborides are profoundly impacted when removed from the lattice, and the diffuse Ce 6*s*-like orbital is stabilized in the cluster relative to the bulk. While the molecular structures determined in this study deviate significantly from bulk CeB<sub>6</sub>, particularly in the structure of the hexaboride unit, there are several notable similarities. Bulk CeB<sub>6</sub>, as with most other *LnB*<sub>6</sub> compounds, is a trivalent material, with each Ce center having a singly occupied 4*f* subshell,<sup>62</sup> a feature that figures prominently in its electronic and magnetic properties. With its highly ionic character, the overall electronic structure of the material has been described as Ce<sup>3+</sup> (B<sub>6</sub>)<sup>3-</sup>,<sup>63</sup> as the neutral molecular units probed in this study. However, with increasing temperature, conductivity increases<sup>64</sup> as electrons are promoted from the B 2*p* orbitals to partially occupy the Ce 5*d* conduction band. In the case of small molecular units, the diffuse Ce 6*s*-based molecular orbital is stabilized relative to the Ce 5*d* orbitals, suggesting that the bulk lattice confines and therefore destabilizes the Ce 6*s* band. This study therefore suggests that on the surface, edges and corners, the lower energy excitations associated with promoting an electron to the 6*s* state, which can readily couple to the detachment continuum because it is diffuse, play a role in the electronic emission properties of this material. The bulk lattice constant

is 4.14 Å, placing the Ce–B<sub>6</sub> center separation at 3.58 Å.<sup>65</sup> In the neutral relaxed teardrop, along the C<sub>s</sub> plane, the average Ce–B internuclear distance is 3.33 Å.

Finally, we compare these results to recently reported studies on similar species. The planar, or near-planar, structure giving rise to the experimental spectrum in this study is nearly identical to the structure tentatively assigned to the spectrum of SmB<sub>6</sub><sup>-</sup> collected by Bowen and coworkers.<sup>21</sup> While the molecular structures of SmB<sub>6</sub><sup>-</sup> and CeB<sub>6</sub><sup>-</sup> in the present work are predicted to be similar, a few key differences emerge in the electronic structure. The B<sub>6</sub> unit carries a different charge between complexes, adopting a B<sub>6</sub><sup>2-</sup> electron configuration in SmB<sub>6</sub><sup>-</sup> and B<sub>6</sub><sup>3-</sup> in CeB<sub>6</sub><sup>-</sup>. Following this, the lanthanoid centers, too, must adopt different oxidation states of Sm<sup>1+</sup> and Ce<sup>2+</sup>. One of the most striking differences between the PE spectra is the origins of the photoelectrons. In SmB<sub>6</sub><sup>-</sup>, all of the photoelectrons originate from 2*p*-based molecular orbitals, leaving Sm in an oxidation state of +1 in both the anion and neutral. For CeB<sub>6</sub><sup>-</sup>, the transition to the ground state neutral very clearly results from detachment of an electron in a Ce-based 6*s*-like molecular orbital, confirmed by the polarization dependence of bands **X** and **x**. Thus, in the neutral monomer, CeB<sub>6</sub> takes on the same ionic character of the bulk material. The Sm center distinctly lacks occupation of its 6*s*-like molecular orbital; though surprising, it has been shown previously that Sm can alter its superconfiguration to favor 4*f* occupancy over 6*s*.<sup>66</sup> The polarization dependence of band **A** in the 3.49 eV PE spectrum of CeB<sub>6</sub><sup>-</sup> does, however, suggest detachment from B-based 2*p*-like orbitals as is seen with SmB<sub>6</sub><sup>-</sup>.

As a point of comparison, the PE spectrum of the incrementally more boron rich PrB<sub>7</sub><sup>-</sup> molecule is consistent with a 4*f*<sup>2</sup> 6*s* electron configuration for the Pr center, which is analogous to the Ce center configuration in CeB<sub>6</sub><sup>-</sup>.<sup>23</sup> And, as with CeB<sub>6</sub><sup>-</sup>, the first transition observed

corresponds to detachment from the  $6s$ -like orbital. In the ground state neutral, both Ce and Pr assume oxidation states of +3, while the  $B_n$  unit maintains its trianionic charge. Subsequent excited neutral states in  $PrB_7$  also correspond to detachment of orbitals with mostly B  $2p$  character. The B-based orbitals, however, are significantly more stabilized compared to  $CeB_6^-$ . Two of the  $2p$  orbitals in  $CeB_6^-$  are only about 1 eV lower in energy than the Ce  $6s$ , with two additional orbitals lying just above the occupied  $4f$  orbital (Fig. 5). In  $PrB_7^-$ , the first occupied  $2p$  orbitals are energetically below the singly occupied  $4f$  orbitals, about 2 eV lower in energy than the  $6s$ . These energetic differences may simply be the result of the different structure favored by  $PrB_7^-$ , in which the  $B_7^{3-}$  ligand adopts a highly symmetric six-membered ring with a central boron atom buckled out-of-plane.

The distorted geometry is reminiscent of the puckered teardrop of  $CeB_6^-$ , but in the case of  $PrB_7^-$ , Pr is located over the center of the ring and directly coordinates every B atom, which may result in better charge stabilization on the  $B_7^{3-}$  ligand. The puckering of the teardrop structure is also interesting when compared with the B-poorer clusters,  $PrB_3^-$  and  $PrB_4^-$ , which are planar.<sup>27</sup> This structural change demonstrates how the stabilization provided by the planarity of anionic boride clusters only begins to be outcompeted by Coulombic stabilization when the clusters approach the stoichiometry of the bulk hexaborides.

## V. CONCLUSIONS

The electronic and molecular structure of the  $CeB_6$  molecular unit has been probed by anion PE spectroscopy and DFT calculations to gain insight into structural and electronic relaxation on edge and corner sites of ionic material. Two competitive molecular structures were identified: an asymmetric boat-like structure and a planar or near-planar teardrop structure. Ce

adopted different superconfigurations between isomers; the boat-like structure had a  $4f$  superconfiguration while the teardrop favored a  $4f6s$  occupancy. The  $B_6$  ligand in these structures carries a charge of -4 and -3, respectively. The teardrop structure, which was calculated to be 0.01 eV higher in energy than the boat structure, was most consistent with the experimental spectrum. The conclusion is that the unique stability of planar  $B_6$  structure<sup>51,61</sup> compensates for the reduced Coulombic stabilization between the Ce cation and  $B_6$  anion in the teardrop structure relative to the boat structure.

From an electronic structure standpoint,  $B_6$ -local orbitals crowd the energy window between the Ce  $4f$  and  $6s$  orbitals. A low-lying transition from the B-based orbitals is observed slightly less than 1eV above the ground state. The transition is embedded in a continuum of detachment signal, which is evocative of the thermal conductivity that is characteristic to the bulk material. However, unlike the bulk, our results suggest that edge and corner conductivity involves stabilized, highly diffuse  $6s$  orbitals or bands rather than the bulk-favored  $5d$  band. Finally, high-spin and open-shell low-spin states were calculated to be very close in energy for both the anion and neutral, a characteristic that reflects how decoupled the  $4f$  electron is from the  $B_6$   $2p$ - and Ce  $6s$ -based molecular orbitals.

## **ASSOCIATED CONTENT**

### **Supporting Information**

All molecular structures and relative energies of  $CeB_6$  anions and neutrals that converged in calculations, optimized geometries of the energetically competitive species, a summary of all simulation parameters, a comparison of the electronic structures of the quartet anion states of the teardrop and near-octahedral (bulk-like) structures, and NTOs of the neutral excited electronic state determined with TD-DFT calculations.

## AUTHOR INFORMATION

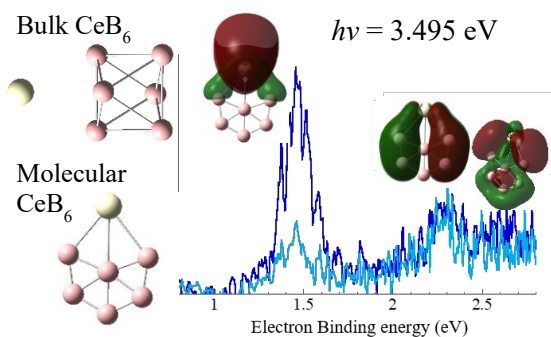
Corresponding Authors

\*E-mail: [cjarrold@indiana.edu](mailto:cjarrold@indiana.edu); [hhratchian@ucmerced.edu](mailto:hhratchian@ucmerced.edu)

## ACKNOWLEDGMENTS

This work was supported by the U.S. Department of Energy, Office of Science, Basic Energy Sciences, CPIMS Program, under award no. DE-FG02-07ER15889 at Indiana University. H.P.H. acknowledges support from the Petroleum Research Fund (ACS-PRF No. 56806-DNI6) and the Hellman Fellows Fund for a faculty fellowship. H.H. and H.P.H. were provided computing time on the Multi-Environment Computer for Exploration and Discovery (MERCED) cluster at UC Merced, which is supported by National Science Foundation Grant No. ACI-1429783. CDH was supported by the National Science Foundation REU Program at IU Chemistry (CHE-1460720). Both C.C.J. and H.P.H. gratefully acknowledge additional support for the multi-institutional collaboration from the IU-MSI STEM Initiative, with funding from the Department of Navy Grant No. N000141512423.

## TOC Graphic



## REFERENCES

- <sup>1</sup> Etourneau, J.; Mercurio, J.P.; Berrada, A.; Hagenmuller, P.; Georges, R.; Bourezg, R.; Gianduzzo, J.C. The Magnetic and Electrical Properties of some Rare Earth Tetraborides. *J. Less-Common Met.* **1979**, *67*, 531-539.
- <sup>2</sup> Schell, G.; Winter, H.; Rietschel, H.; Gompf, F. Electronic Structure and Superconductivity in Metal Hexaborides. *Phys. Rev. B* **1982**, *25*, 1589-1599.
- <sup>3</sup> Jie, D.; Tong, Z.; Li, Z.; Ji-Guang, D.; Gang, J.; Hong-Bin, W. Elastic Properties and Electronic Structures of Lanthanide Hexaborides. *Chin. Phys. B* **2015**, *24*, 096201 1-9.
- <sup>4</sup> Barrow, R.F.; Clements, R.M.; Harris, S.M.; Jenson, P.P. Electronic Spectrum of Gaseous CeO *Astrophys. J.* **1979**, *229*, 439-447.
- <sup>5</sup> Linton, C.; Dulick, M.; Field, R.W.; Carette, P.; Leyland, P.C.; Barrow, R.F. Electronic States of the CeO Molecule, Absorption, Emission and Laser Spectroscopy. *J. Mol. Spec.* **1983**, *102*, 441-497.
- <sup>6</sup> Dulick, M.; Field, R.W. Electronic Structure of PrO- An Analysis Summary *J. Mol. Spec.* **1985**, *113*, 105-141.
- <sup>7</sup> McDonald, S.A.; Rice, S.F.; Field, R.W.; Linton, C. Laser Spectroscopy of Low-Lying Excited States in YbO- Linkage of the Yb<sup>2+</sup> f<sup>13</sup>s and f<sup>14</sup> Configurations. *J. Chem. Phys.* **1990**, *93*, 7676-7686.
- <sup>8</sup> Carette, P. The Ultraviolet Emission Spectrum of LaO. *J. Mol. Spec.* **1990**, *140*, 269-279.
- <sup>9</sup> Linton, C.; Dulick, M.; Field, R.W.; Carette, P.; Barrow, R.F. Low-Lying Electronic States of CeO. *J. Chem. Phys.* **1981**, *74*, 189-191.
- <sup>10</sup> Klingeler, R.; Pontius, N.; Luttgens, G.; Bechtold, P.S.; Neeb, M.; Eberhardt, W. Photoelectron Spectroscopy of GdO<sup>-</sup>. *Phys. Rev. A* **2002**, *65*, 032502 1-3.
- <sup>11</sup> Kafader, J.O.; Ray, M.; Jarrold, C.C. Photoelectron Spectrum of PrO<sup>-</sup>. *J. Chem. Phys.* **2015**, *143*, 064305 1-6.
- <sup>12</sup> Heaven, M.C. Probing Actinide Electronic Structure using Fluorescence and Multi-Photon Ionization Spectroscopy. *Phys. Chem. Chem. Phys.* **2006**, *8*, 4497-4509.
- <sup>13</sup> Kafader, J.O.; Ray, M.; Jarrold, C.C. Low-Lying Electronic Structure of EuH, EuOH, and EuO Neutrals and Anions Determined by Anion Photoelectron Spectroscopy and DFT Calculations. *J. Chem. Phys.* **2015**, *142*, 034305 1-9.

- <sup>14</sup> Ray, M.; Felton, J.A.; Kafader, J.O.; Topolski, J.E.; Jarrold, C.C. Photoelectron Spectra of CeO<sup>-</sup> and Ce(OH)<sub>2</sub><sup>-</sup>. *J. Chem. Phys.* **142**, 064305 1-8 (2015).
- <sup>15</sup> Bujin, G.; Linton, C. High Resolution Analysis of Transitions to the Five Lowest Electronic States of Samarium Monoxide. *J. Mol. Spec.* **1989**, *137*, 114-126.
- <sup>16</sup> Kaledin, L.A.; McCord, J. E.; and Heaven, M.C. Laser Spectroscopy of CeO- Characterization and Assignment of States in the 0 – 3 eV Range. *J. Mol Spec.* **1993**, *158*, 40-61.
- <sup>17</sup> Kulikov, A.N.; Kaledin, L.A.; Kobylansky, A.I.; Gurvich, L.V. Dye laser and thermal emission spectroscopy of the TbO molecule. *Can. J. Phys.* **1984**, *62*, 1855-1879.
- <sup>18</sup> Kaledin, L.A.; Linton, C.; Clarke, T.E.; Field, R.W. Laser Spectroscopy of the Lanthanide Monofluorides- The Ground State Configuration of Holmium Fluoride. *J. Mol. Spec.* **1992**, *154*, 417-426.
- <sup>19</sup> Field, R.W. Diatomic Molecular Electronic Structure beyond Simple Molecular Constants. *Ber. Bunsenges. Phys. Chem.* **1982**, *86*, 771-779.
- <sup>20</sup> Klingeler, R.; Lüttgens, G.; Pontius, N.; Rochow, R.; Bechtold, P.S.; Neeb, M.; Eberhardt, W. Photoelectron Spectra of Small LaO<sub>n</sub><sup>-</sup> Clusters: Decreasing Electron Affinity upon Increasing the Number of Oxygen Atoms. *Eur. Phys. J. D* **1999**, *9*, 263-267.
- <sup>21</sup> Robinson, P.F.; Zhang, X.; McQueen, T.; Bowen, K.H.; Alexandrova, A.N. SmB<sub>6</sub><sup>-</sup> Cluster Anion: Covalency Involving f Orbitals. *J. Phys. Chem. A* **2017**, *121*, 1849-1854.
- <sup>22</sup> Mason, J.L.; Harb, H.; Topolski, J.E.; Hratchian, H.P.; Jarrold, C.C. A Tale of Two Stabilities: How One Boron Atom Affects a Switch in Bonding Motifs in CeO<sub>2</sub>B<sub>x</sub> (x = 2, 3) Complexes. *J. Phys. Chem. A* **2018**, *122*, 9879-9885.
- <sup>23</sup> Chen, T.-T.; Li, W.-L.; Jian, T.; Chen, X.; Li, J.; Wang, L.-S. PrB<sub>7</sub><sup>-</sup>: A Praseodymium-Doped Boron Cluster with a Pr<sup>II</sup> Center Coordinated by a Doubly Aromatic Planar η<sup>7</sup>-B<sub>7</sub><sup>3-</sup> Ligand. *Angew. Chem.* **2017**, *129*, 7020-7024.
- <sup>24</sup> Li, W.-L.; Chen, T.-T.; Xing, D.-H.; Chen, X.; Li, J.; Wang, L.-S. Observation of Highly Stable and Symmetric Lanthanide Octa-boron Inverse Sandwich Complexes. *Proc. Nat. Acad. Sci.* **2018**, *115*, E6972-E6977.
- <sup>25</sup> Cheng, S.-B.; Berkdemir, C.; Castleman, Jr., A.W. Observation of d-p Hybridized Aromaticity in Lanthanum-doped Boron Clusters. *Phys. Chem. Chem. Phys.* **2014**, *16*, 533-539.
- <sup>26</sup> Chen, T. T.; Li, W. L.; Li, J.; Wang, L. S., [La(η<sup>x</sup>-B<sub>x</sub>)La]<sup>-</sup> (x = 7-9): A New Class of Inverse Sandwich Complexes. *Chem. Sci.* **2019**, DOI: 10.1039/C8SC05443F

- <sup>27</sup> Chen, X.; Chen, T. T.; Li, W. L.; Lu, J. B.; Zhao, L. J.; Jian, T.; Hu, H. S.; Wang, L. S.; Li, J., Lanthanides with Unusually Low Oxidation States in the  $\text{PrB}_3^-$  and  $\text{PrB}_4^-$  Boride Clusters. *Inorg. Chem.* **2019**, *58*, 411-418.
- <sup>28</sup> Kitsopoulos, T.N.; Chick, C.J.; Zhao, Y.; Neumark, D.M. Threshold Photodetachment Spectroscopy of  $\text{C}_5^-$ . *J. Chem. Phys.* **1991**, *95*, 5479-
- <sup>29</sup> Arnold, C.C.; Neumark, D.M. The Study of Small Carbon and Silicon Clusters using Negative Ion Photodetachment Techniques, in *Advances in Metal and Semiconductor Clusters*, Vol. III, Edited by M. Duncan, JAI Press, Greenwich, **1994**, 113-148.
- <sup>30</sup> Raghavachari, K.; Rohlfing, C.M. Electronic Structures of the Negative Ions  $\text{Si}_2 - \text{Si}_{10}$ , Electron Affinities of Small Silicon Clusters. *J. Chem. Phys.* **1991**, *94*, 3670-3678.
- <sup>31</sup> Kitsopoulos, T.N.; Chick, C.J.; Weaver, A.; Neumark, D.M. Vibrationally Resolved Photoelectron Spectra of  $\text{Si}_3^-$  and  $\text{Si}_4^-$ . *J. Chem. Phys.* **1990**, *93*, 6108 – 6110.
- <sup>32</sup> Rothgeb, D.W.; Mann, J.E.; Waller, S.E.; Jarrold, C.C. Structures of Trimetallic Molybdenum and Tungsten Suboxide Cluster Anions *J. Chem. Phys.* **2011**, *135*, 104312 1-12.
- <sup>33</sup> Yoder, B.L.; Maze, J.T.; Raghavachari, K.; Jarrold, C.C. Structures of  $\text{Mo}_2\text{O}_y^-$  and  $\text{Mo}_2\text{O}_y$  ( $y = 2, 3$ , and 4) Studied by Anion Photoelectron Spectroscopy and Density Functional Theory Calculations. *J. Chem. Phys.* **2005**, *122*, 094313 1-9.
- <sup>34</sup> Saha, A.; Raghavachari, K. Hydrogen Evolution from Water through Metal Sulfide Reactions. *J. Chem. Phys.* **2013**, *139*, 2043011-12.
- <sup>35</sup> Alexandrova, A.N.; Boldyrev, A.I.; Zhai, H.-J.; Wang, L.-S. Photoelectron Spectroscopy and *ab initio* Study of the Doubly Antiaromatic  $\text{B}_6^{2-}$  Dianion, in the  $\text{LiB}_6^-$  cluster, *J. Chem. Phys.* **2005**, *122*, 054313 1-8.
- <sup>36</sup> Moravec, V. D.; Jarrold, C. C. Study of the Low-lying States of  $\text{NiO}^-$  and  $\text{NiO}$  Using Anion Photoelectron Spectroscopy. *J. Chem. Phys.* **1998**, *108*, 1804-1810.
- <sup>37</sup> Waller, S. E.; Mann, J. E.; Jarrold, C. C. Asymmetric Partitioning of Metals among Cluster Anions and Cations Generated via Laser Ablation of Mixed Aluminum/Group 6 Transition Metal Targets. *J. Chem Phys. A* **2013**, *117*, 1765-1772.
- <sup>38</sup> Dietz, T. G.; Duncan, M. A.; Powers, D. E.; Smalley, R. E. Laser Production of Supersonic Metal Cluster Beams. *J. Chem. Phys.* **1981**, *74*, 6511-6512.

- <sup>39</sup> Frisch, M. J.; Trucks, G. W.; Schlegel, H. B.; Scuseria, G. E.; Robb, M. A.; Cheeseman, J. R.; Scalmani, G.; Barone, V.; Mennucci, B.; Petersson, G. A.; et al, GAUSSIAN 16, Gaussian Inc., Wallingford, CT, USA, 2016.
- <sup>40</sup> Frisch, M. J.; Trucks, G. W.; Schlegel, H. B.; Scuseria, G. E.; Robb, M. A.; Cheeseman, J. R.; Scalmani, G.; Barone, V.; Petersson, G. A.; Nakatsuji, H.; et al, Gaussian Development Version, Revision I.10+, Gaussian, Inc., Wallingford CT, USA, 2016.
- <sup>41</sup> Cao, X.; Dolg, M. Valence Basis Sets for Relativistic Energy-consistent Small-core Lanthanide Pseudopotentials. *J. Chem. Phys.* **2001**, *115*, 7348-7355.
- <sup>42</sup> Dunning, T. H. Gaussian Basis Sets for use in Correlated Molecular Calculations. I. The Atoms Boron Through Neon and Hydrogen. *J. Chem. Phys.* **1989**, *90*, 1007-1023.
- <sup>43</sup> Thompson, L. M. ; Harb, H.; Hratchian, H. P. Natural Ionization Orbitals for Interpreting Electron Detachment Processes. *J. Chem. Phys.* **2016**, *144*, 204117.
- <sup>44</sup> Seeger, R.; Pople, J. A. Self-consistent Molecular Orbital Methods. XVIII. Constraints and Stability in Hartree-Fock Theory. *J. Chem. Phys.* **1977**, *66*, 3045-3050.
- <sup>45</sup> Bauernschmitt, R.; Ahlrichs, R. Stability Analysis for Solutions of the Closed Shell Kohn-Sham Equation. *J. Chem. Phys.* **1996**, *104*, 9047-9053.
- <sup>46</sup> Bauernschmitt, R.; Ahlrichs, R. Treatment of Electronic Excitations Within the Adiabatic Approximation of Time Dependent Density Functional Theory. *Chem. Phys. Lett.* **1996**, *256*, 454-464.
- <sup>47</sup> Furche, F.; Ahlrichs, R. Adiabatic Time-dependent Density Functional Methods for Excited State Properties. *J. Chem. Phys.* **2002**, *117*, 7433-7447.
- <sup>48</sup> Martin, R. L. Natural Transition Orbitals. *J. Chem. Phys.* **2003**, *118*, 4775-4777.
- <sup>49</sup> Schaugaard, R.N.; Topolski, J.E.; Ray, M.; Raghavachari, K.; Jarrold, C.C. Insight into Ethylene Interactions with Molybdenum Suboxide Cluster Anions from Photoelectron Spectra of Chemifragments. *J. Chem. Phys.* **2018**, *148*, 054308 1-13.
- <sup>50</sup> O'Malley, S. M.; Beck, D. R.; Calculation of  $Ce^-$  Binding Energies by Analysis of Photodetachment Partial Cross Sections. *Phys. Rev. A* **2006**, *74*, 042509 1-10.
- <sup>51</sup> Alexandrova, A.N.; Boldyrev, A.I.; Zhai, H.-J.; Wang, L.-S.; Steiner, E.; Fowler, P.W. Structure and Bonding in  $B_6^-$  and  $B_6$ : Planarity and Antiaromaticity. *J. Phys. Chem. A* **2003**, *107*, 1359-1369.
- <sup>52</sup> Romanescu, C.; Sergeeva, A. P.; Li, W. L.; Boldyrev, A. I.; Wang, L. S., Planarization of  $B_7^-$  and  $B_{12}^-$  Clusters by Isoelectronic Substitution:  $AlB_6^-$  and  $AlB_{11}^-$ . *J. Am. Chem. Soc.* **2011**, *133*, 8646-8653.

- <sup>53</sup> Sonnenberg, J. L.; Hratchian, H. P.; Schlegel, H. B. Spin Contamination in Inorganic Chemistry Calculations, In *Computational Inorganic and Bioinorganic Chemistry*, Solomon, E. I.; King, R. B.; Scott, R. A., Eds.; Wiley: Chichester, U.K.; 2009, 173-186.
- <sup>54</sup> Waller, S. E.; Mann, J. E.; Rothgeb, D. W.; Jarrold, C. C. Study of MoNbO<sub>y</sub> (y = 2–5) Anion and Neutral Clusters Using Photoelectron Spectroscopy and Density Functional Theory Calculations: Impact of Spin Contamination On Single Point Calculations. *J. Phys. Chem. A* **2012**, *116*, 9639-9652.
- <sup>55</sup> Thompson, L. M.; Hratchian, H. P. Modeling the Photoelectron Spectra of MoNbO<sub>2</sub><sup>-</sup> Accounting for Spin Contamination in Density Functional Theory. *J. Phys. Chem. A* **2015**, *119*, 8744-8751.
- <sup>56</sup> Yamaguchi K.; Jensen, F.; Dorigo, A.; Houk, K. N. A Spin Correction Procedure for Unrestricted Hartree-Fock and Møller-Plesset Wavefunctions for Singlet Diradicals And Polyradicals. *Chem. Phys. Lett.* **1988**, *149*, 537-542.
- <sup>57</sup> Kitagawa, Y.; Saito, T.; Ito, M.; Shoji, M.; Koizumi, K.; Yamanaka, S.; Kawakami, T.; Okumura, M.; Yamaguchi, K. Approximately Spin-Projected Geometry Optimization Method and Its Application to Di-Chromium Systems. *Chem. Phys. Lett.* **2007**, *442*, 445-450.
- <sup>58</sup> Hratchian, H. P. An Efficient Analytic Gradient Theory for Approximate Spin Projection Methods. *J. Chem. Phys.* **2013**, *138*, 101101.
- <sup>59</sup> Thompson, L. M.; Hratchian, H. P. Second Derivatives for Approximate Spin Projection Methods. *J. Chem. Phys.* **2015**, *142*, 054106.
- <sup>60</sup> Thompson, L. M.; Hratchian, H. P. On Approximate Projection Models. *Mol. Phys.* **2018**, in press.
- <sup>61</sup> Li, W.-L.; Chen, X.; Jian, T.; Chen, T.-T.; Li, J.; Wang, L.-S. From Planar Boron Clusters to Borophenes and Metalloborophenes, *Nat. Rev. Chem.* **2017**, *1*, 1-9.
- <sup>62</sup> Liu, L.; Yiu, Y.-M.; Sham, T.-K. Electronic Structures of LaB<sub>6</sub> and CeB<sub>6</sub> Single Crystals: X-ray Absorption Near-edge Structure Studies at the B K-edge and the La and Ce Giant Resonance. *J. Elect. Spec. and Rel. Phenom.* **2011**, *184*, 188-191.
- <sup>63</sup> Makita, R.; Tanaka, K.; Onuki, Y. 5d and 4f Electron Configuration of CeB<sub>6</sub> at 340 and 535 K. *Acta Cryst. B* **2008**, *64*, 534-549.
- <sup>64</sup> Peysson, Y.; Ayache, C.; Salce, B.; Kunii, S.; Kasuya, T. Thermal Conductivity of CeB<sub>6</sub> and LaB<sub>6</sub>. *J. Mag. and Mag. Mat.* **1986**, *59*, 33-40.
- <sup>65</sup> Lüthi, B.; Blumenröder, S.; Hillebrands, B.; Zirngiebl, E.; Güntherodt, G.; Winzer, K. Elastic and Magnetoelastic Effects in CeB<sub>6</sub>. *J. Magn. Magn. Mater.* **1985**, *58*, 321–322.

<sup>66</sup> Topolski, J. E.; Kafader, J. O.; Marrero-Colon, V.; Iyengar, S. S.; Hratchian, H. P.; Jarrold, C. C. Exotic Electronic Structures of  $\text{Sm}_x\text{Ce}_{3-x}\text{O}_y$  ( $x = 0-3$ ;  $y = 2-4$ ) Clusters, and the Effect of High Neutral Density of Low-lying States on Photodetachment Transition Intensities. *J. Chem. Phys.* **2018**, *149*, 054305.

## Figure Captions

**Figure 1.** PE spectra of  $\text{CeB}_6^-$  measured with (a) 2.330 eV and (b) 3.495 eV photon energies. Laser polarizations relative to direction of electron collection is indicated.

**Figure 2.** Calculated relative energies of anion and neutral  $\text{CeB}_6$  structures and spin states. Open shell low spin states are indicated with dashed lines

**Figure 3.** (a) Spectral simulations based on the asymmetric boat structure, (b) planar teardrop structure, and (c) buckled (relaxed) teardrop structure. (d) and (e) show the simulated spectra from (b) and (c), respectively, shifted to lower  $e^-BE$  to overlap with the observed spectra.

**Figure 4.** NIO's for the one-electron allowed transitions associated with the (a) boat and (b) teardrop structures of  $\text{CeB}_6^-$ .

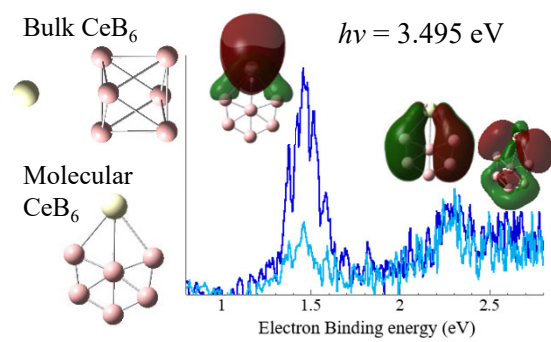
**Figure 5.** Schematic showing the relative orbital energies of  $\text{CeB}_6^-$ ,  $\text{Ce}(\text{B}_3\text{O}_2)^-$  [Ref. 22],  $\text{Ce}(\text{BO})_2^-$  [Ref. 22] and  $\text{CeO}^-$  [Ref. (14)]. Orange lines indicate B  $2p$ -based MOs, the blue lines indicate O  $2p$ -based orbitals, and red lines indicate Ce  $4f$  orbitals. Orbitals that are singly occupied are indicated with lines that are half the width of those representing doubly occupied orbitals.

Table 1. Summary of lowest energy structures and electronic states for  $\text{CeB}_6^-$  and  $\text{CeB}_6$ , in order of decreasing energy.

	Symmetry	General electronic description	$\langle S^2 \rangle$	Relative energy/eV	ADE/eV
<b><math>\text{CeB}_6</math></b>					
Sym. boat ${}^3\text{B}_1$	$\text{C}_{2v}$	$\text{Ce}^{3+}(4f)[\text{B}_6({}^2\text{A})]^{3-}$	2.01	2.18	1.61
Asym. boat ${}^3\text{A}$	$\text{C}_1$	$\text{Ce}^{3+}(4f)[\text{B}_6({}^2\text{A})]^{3-}$	2.04	1.76	1.76
Asym. boat ${}^1\text{A}$	$\text{C}_1$	$\text{Ce}^{3+}(4f)[\text{B}_6({}^2\text{A})]^{3-}$	1.03	1.74	1.74
Planar teardrop <sup>a</sup> ${}^3\text{A}_1$	$\text{C}_{2v}$	$\text{Ce}^{3+}(4f)[\text{B}_6({}^2\text{A}_2)]^{3-}$	2.01	1.57	1.56 (1.53) <sup>b</sup>
Planar teardrop <sup>a</sup> ${}^1\text{A}_1$	$\text{C}_{2v}$	$\text{Ce}^{3+}(4f)[\text{B}_6({}^1\text{A}_2)]^{3-}$	0.99	1.56	1.52
Buckled teardrop ${}^1\text{A}''$	$\text{C}_s$	$\text{Ce}^{3+}(4f)[\text{B}_6({}^1\text{A}_2)]^{3-}$	1.02	1.53	1.49
Buckled teardrop ${}^3\text{A}''$	$\text{C}_s$	$\text{Ce}^{3+}(4f)[\text{B}_6({}^2\text{A}'')]^{3-}$	2.01	1.53	1.52 (1.48) <sup>b</sup>
<b><math>\text{CeB}_6^-</math></b>					
Bulk monomer ${}^4\text{A}$	$\text{C}_1$	$\text{Ce}^{2+}(4f6s)[\text{B}_6({}^2\text{A})]^{3-}$	3.88	1.96	
Sym. boat ${}^2\text{A}_1$	$\text{C}_{2v}$	$\text{Ce}^{2+}(4f_{b1} 5d_{b1})[\text{B}_6({}^2\text{A}_1)]^{3-}$	1.77	0.73	
Sym. boat ${}^4\text{B}_1$	$\text{C}_{2v}$	$\text{Ce}^{2+}(4f_{a1} 5d_{b1})[\text{B}_6({}^2\text{A}_1)]^{3-}$	3.77	0.57	
Asym. boat ${}^4\text{A}$	$\text{C}_1$	$\text{Ce}^{2+}(4f6s)[\text{B}_6({}^2\text{A})]^{3-}$	3.78	0.51	
Teardrop ${}^2\text{B}_2$	$\text{C}_{2v}$	$\text{Ce}^{2+}(4f6s)[\text{B}_6({}^2\text{A}_2)]^{3-}$	1.76	0.05	
Teardrop ${}^2\text{A}_1$	$\text{C}_{2v}$	$\text{Ce}^{2+}(4f6s)[\text{B}_6({}^2\text{A}_2)]^{3-}$	1.74	0.04	
Teardrop ${}^4\text{A}_2$	$\text{C}_{2v}$	$\text{Ce}^{2+}(4f6s)[\text{B}_6({}^2\text{A}_2)]^{3-}$	3.76	0.01	
Asym. boat ${}^2\text{A}$	$\text{C}_1$	$\text{Ce}^{3+}(4f)[\text{B}_6({}^1\text{A})]^{4-}$	0.76	0.0	

<sup>a</sup> One imaginary frequency

<sup>b</sup> ADE for transition from  ${}^2\text{A}_1$  excited state.



TOC Graphic.

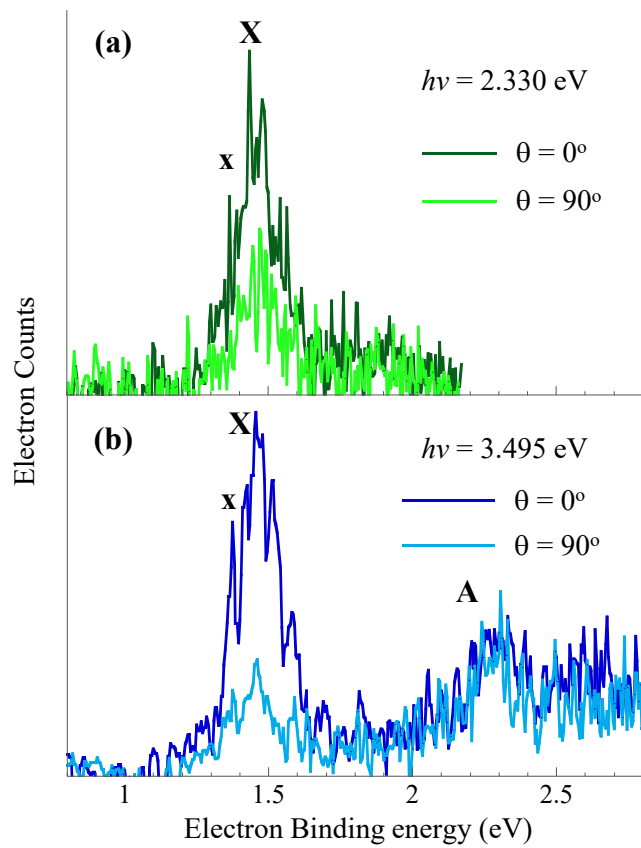


Figure 1. Mason et al.

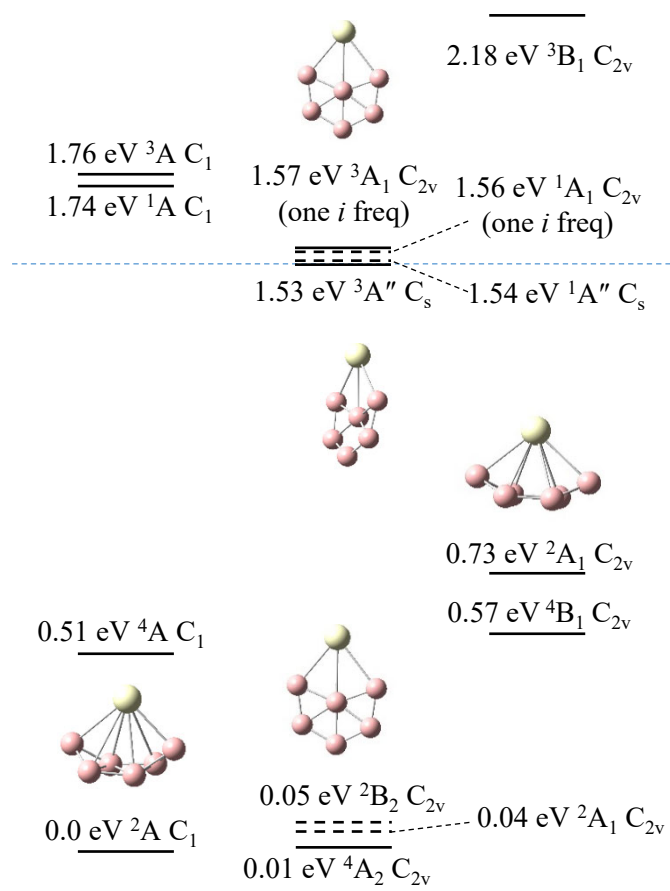


Figure 2. Mason et al.

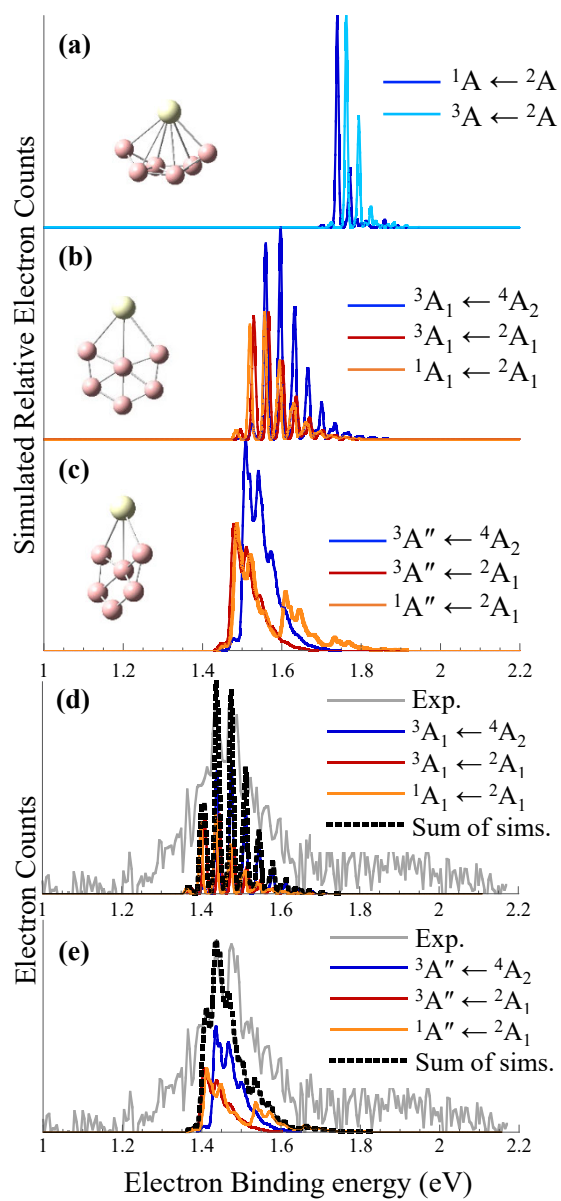
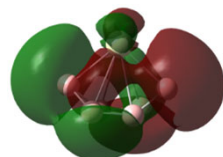


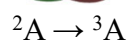
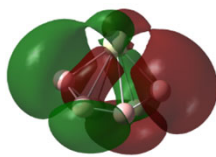
Figure 3. Mason et al.

(a) Boat Structure

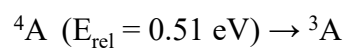
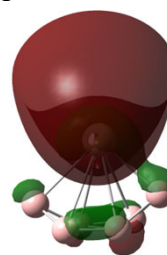
Alpha Detachment



Beta Detachment

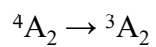
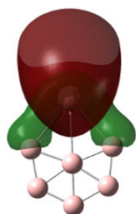


Alpha Detachment

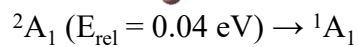
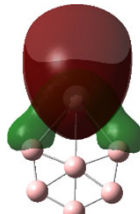


(b) Teardrop Structure

Alpha Detachment



Alpha Detachment



Alpha Detachment

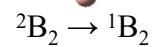
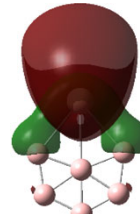


Figure 4. Mason et al.

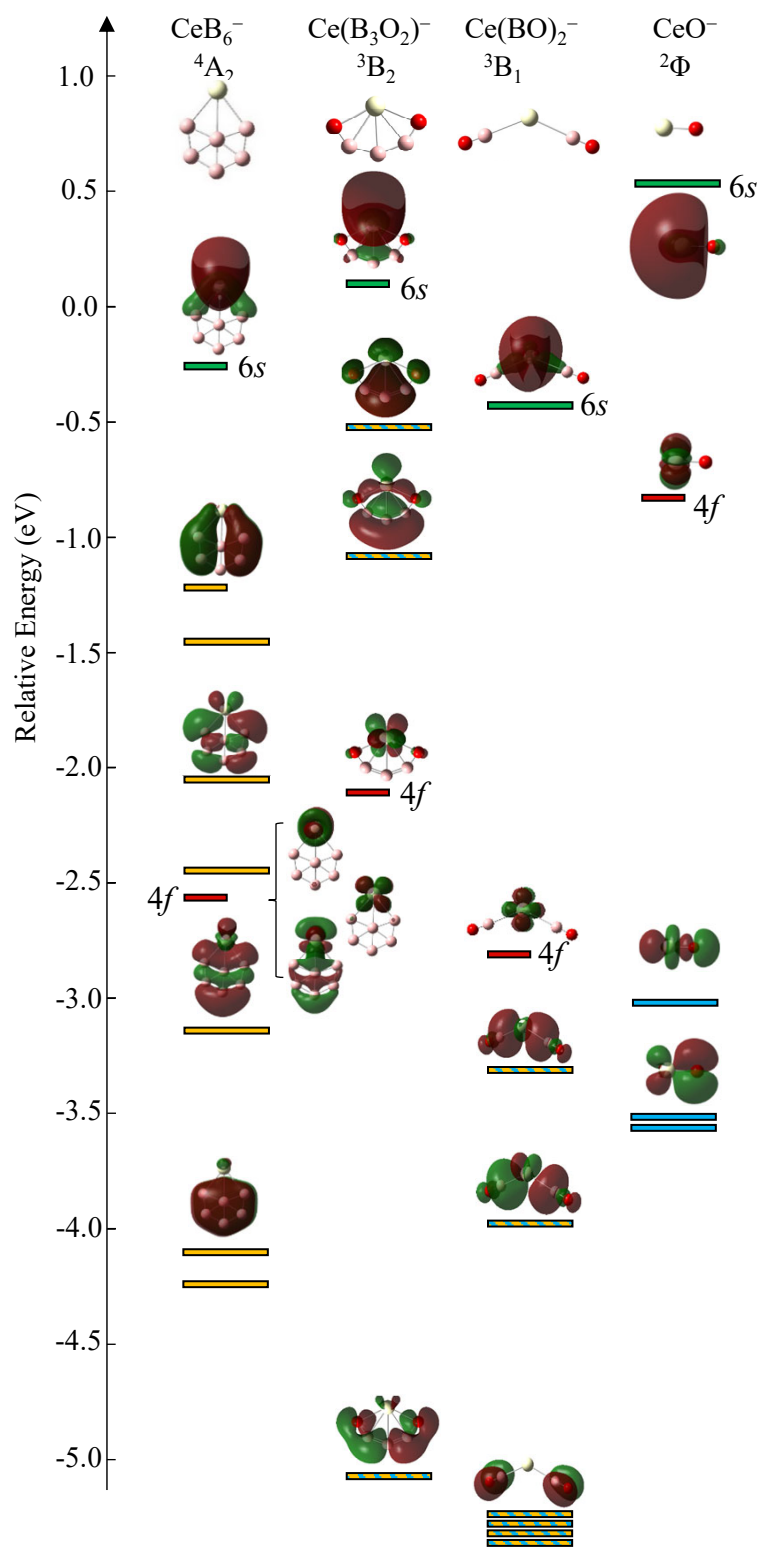


Figure 5. Mason et al.